HHS Public Access

Author manuscript

Microrna. Author manuscript; available in PMC 2018 January 01.

Published in final edited form as:

Microrna. 2017 ; 6(2): 143–150. doi:10.2174/2211536605666161109111031.

MicroRNA-130a Regulation of Desmocollin 2 in a Novel Model of Arrhythmogenic Cardiomyopathy

Stefan R. Mazurek, **Tyler Calway**, **Cynthia Harmon**, **Priyanka Farrell**, and **Gene H. Kim***

Department of Medicine, University of Chicago, Chicago, United States

Abstract

Background—MicroRNAs are small noncoding RNA molecules that play a critical role in regulating physiological and disease processes. Recent studies have now recognized microRNAs as an important player in cardiac arrhythmogenesis. Molecular insight into arrhythmogenic cardiomyopathy (AC) has primarily focused on mutations in desmosome proteins. To our knowledge, models of AC due to microRNA dysregulation have not been reported. Previously, we reported on miR-130a mediated down-regulation of Connexin43.

Objective—Here, we investigate miR-130a-mediated translational repression of Desmocollin2 (DSC2), as it has a predicted target site for miR-130a. DSC2 is an important protein for cell adhesion, which has been shown to be dysregulated in human AC.

Results—After induction of miR-130a, transgenic mice demonstrated right ventricular dilation. Surface ECG revealed spontaneous premature ventricular complexes confirming an arrhythmogenic phenotype in αMHC-miR130a mice. Using total protein from whole ventricular lysate, western blot analysis demonstrated an 80% reduction in DSC2 levels in transgenic myocardium. Furthermore, immunofluorescent staining confirmed downregulation of DSC2 in transgenic compared with littermate control myocardium. In transgenic hearts, histologic findings revealed fibrosis and lipid accumulation within both ventricles. To validate DSC2 as a direct target of miR-130a, we performed *in vitro* target assays in 3T3 fibroblasts, known to express miR-130a. Using a luciferase reporter fused to the 3′UTR of DSC2 compared with a control, we found a 42% reduction in luciferase activity with the DSC2 3′UTR. This reduction was reversed upon selective inhibition of miR-130a.

Conclusion—Overexpression of miR-130a results in a disease phenotype characteristic of AC and therefore, may serve as potential model for microRNA-induced AC.

Keywords

Arrhythmia; cardiomyopathy; desmocollin 2; desmosome; intercalated disc; miR-130a

*Address correspondence to this author at the Department of Medicine, University of Chicago, Chicago, United States; Tel: 773-834-1392; Fax: 773-834-1764; gkim1@medicine.bsd.uchicago.edu.

CONFLICT OF INTEREST

The authors confirm that this article content has no conflict of interest.

1. INTRODUCTION

Arrhythmogenic cardiomyopathy (AC) is most commonly characterized as a disease of the intercalated disc that promotes abnormal cardiac conduction [1]. Clinically, AC is frequently referred to as arrhythmogenic right ventricular cardiomyopathy/dysplasia (ARVC/D). However, clinical reports have now defined AC to encompass a broader phenotypic spectrum; with the identification of left-dominant and biventricular subtypes [2, 3]. Unlike idiopathic dilated cardiomyopathy (DCM), AC typically presents an arrhythmogenic burden that exceeds the degree of cardiac dysfunction defined by morphology, histology, and ejection fraction [4]. Heterogeneity of the disease phenotype, however, can often lead to clinical misdiagnosis as DCM [5].

AC manifests as electrical and mechanical uncoupling of the ventricular myocardium. Ultimately, the structural changes underlying the disease promote ventricular tachyarrhythmias, sudden cardiac death, and heart failure [6]. It is diagnosed clinically using electrocardiogram (ECG) and morphological recordings in conjunction with genetic screening and familial disease history. However, histological evidence for transmural fibrofatty replacement remains the gold standard for diagnosis [7, 8]. Approximately half of all AC cases can be attributed to inherited mutations, which most commonly occur in genes encoding desmosomal proteins [9]. In cardiac tissue, desmosomes create strong myocyte-myocyte interactions at the intercalated disc. Along with their association with fascia adherens proteins, desmosomal proteins provide stability and mechanical continuity to the myocardium. Furthermore, desmosomes localize and interact with connexins, which are essential for fast electrical propagation of the action potential [10]. Recent evidence has suggested that desmosomal dysfunction is associated with diminished connexin43 expression at the intercalated disc [11].

Given that many mutations associated with AC are non-sense or frame-shift mutations of desmosomal genes, haploinsufficiency of desmosomal proteins has been proposed as one of the potential mechanisms that underlie the progression of dilated cardiomyopathy with a predominant ventricular arrhythmia burden [12, 13]. In fact, downregulation of desmosomal proteins have been described in dilated cardiomyopathy patients with and without known genetic mutations [14, 15]. These results suggest that other non-genetic factors may be contributing to downregulation of desmosomal proteins that promote desmosomal dysfunction.

Studies investigating the molecular mechanisms of AC have mainly focused on the genetic mutations that cause desmosomal dysfunction. To our knowledge, no models of AC have been described involving microRNAs as a potential mechanism for desmosomal dysfunction. Previously, our laboratory characterized cardiac arrhythmogenesis and ventricular dysfunction with inducible overexpression of the microRNA-130a-3p (miR-130a) in a cardiac-specific transgenic mouse. We found that miR-130a mediated down-regulation of Connexin43, which likely created a substrate for both inducible and spontaneous ventricular arrhythmias [16].

The pathogenesis of cardiac arrhythmias can be mostly attributed to dysregulation of ion channels and pumps, abnormal intracellular Ca^{2+} handling, and disrupted cell-cell electrical coupling. Recent studies have highlighted the importance of microRNAs as regulators for many of the aforementioned disease processes [17]. MicroRNAs are small noncoding RNAs that play an important physiological role in the regulation of gene expression. Over the past few decades, a vast number of microRNAs have been shown to play a role in a variety of disease phenotypes, including cardiovascular disease. The selective binding of microRNAs to the target mRNA characteristically leads to repression of protein translation and, potential destabilization and degradation of the target mRNA. MicroRNAs associate with mRNA by binding complementary nucleotide sequences within the 3′ untranslated region (3′ UTR) or protein-coding regions of mRNA transcripts [17, 18]. These “target sites” are typically well conserved throughout mammalian species. Gene regulation by microRNAs provides for finely tuned control over complex genetic pathways. In the event that microRNA levels become aberrant, pathophysiological conditions can result.

Our lab previously described a regulatory role for connexin 43 expression in the myocardium by miR-130a. However, the gene regulatory role of miR-130a in cardiovascular function is still not well defined. Previous studies have shown miR-130a to be upregulated in myocardium of patients with heart failure [19, 20]. Furthermore, our recent analysis of heart failure patient samples found that miR-130a is significantly upregulated in patients who exhibited ventricular arrhythmias [21]. In this study, we investigated miR-130a regulation of Desmocollin 2 (DSC2) gene expression, as it has a predicted target site for miR-130a. DSC2 is an important desmosomal protein that has been shown to be dysregulated in human arrhythmogenic cardiomyopathy [15, 22, 23]. The results from this study show that overexpression of miR-130a promotes an AC disease phenotype. The data also suggest that DSC2 is a direct target of miR-130a, contributing to desmosomal dysfunction and potentially the AC phenotype.

2. MATERIALS AND METHODS

2.1. Transgenic αMHC-miR-130a Mice

All procedures were approved by and performed in accordance with the University of Chicago Institutional Animal Care and Use Committee. αMHC-tTA/TetO-miR130a mice (referred to as “αMHC-mir130a mice”) were generated as described in Osbourne *et al.* [16].

2.2. Transthoracic Echocardiography

Mice were anesthetized with 1–2% isoflurane in 700 ml O_2/min *via* a facemask. Temperature was monitored and maintained at 37°C using a heat pad and heat lamp. Heart rate was maintained at 400–450 bpm. Anesthetized mice were placed on a temperature-controlled platform and echocardiography was performed using a Vevo770 ultrasound system (VisualSonics Inc.; Toronto, Canada). An echocardiographer blind to animal genotype captured in B-mode.

2.3. Surface ECG

Electrocardiograms (ECG) on anesthetized mice (as previously described above) were obtained from needle electrodes inserted subcutaneously into each limb. Multiple leads were recorded for 3 min at 2 MHz. Electrocardiographic signals were amplified with an ECG Bioamplifier (AD Instruments; Colorado Springs, CO), converted from analog to digital with an ACQ-16 Acquisition Interface and recorded with Ponemah Physiology Platform software (Gould; Valley View, OH). Recordings were analyzed using the ECG module of LabChart 5 software (AD Instruments).

2.4. Histology

Hearts were harvested at the time points specified and flash frozen in Tissue-Tek OCT compound (Electron Microscopy Sciences; Hatfield, PA) using liquid nitrogen. Frozen hearts were sectioned at 12 μm thickness. For Picro-Sirius Red: Sections were incubated Picro-Sirius Red solution and then rinsed with 0.5% acetic acid and 100% ethanol, sequentially. For Oil Red O: Sections were fixed with 4% PFA and rinsed with 60% isopropanol, and then incubated with freshly filtered Oil Red O solution at room temperature. Sections were mounted with VECTASHIELD® Mounting Media with DAPI (Vector Laboratories; Burlingame, CA), and visualized with ProGres Capture Pro Software (Jenoptik; Jena, Germany) using a Leica DM2000 microscope equipped with a Jenoptik ProgRes C14plus camera.

2.5. Luciferase Assay

NIH 3T3 cells were cultured with DMEM (Gibco; Waltham, MA) supplemented with 10% fetal bovine serum, 1% penicillin/streptomycin, and maintained at 37°C with 5% CO_2 and 95% humidity.

For transfection, 3–5 × 10^5 cells were plated per well and transfected using Lipofectamine 3000 (Thermo Fisher Scientific, Waltham, MA) with 1 μg pMT01 (control vector), or DSC2 3′ UTR reporter (GeneCopoeia; Rockville, MD); which contain both firefly and renilla luciferase reporters. Luciferase activities were measured (Promega Glomax®-20/20 Luminometer) using the Dual Luciferase Reporter Assay System (Genecopia) with firefly luciferase activities calculated as the mean ± SD after being normalized by renilla luciferase activities. For inhibitor assays: a miR-CURY LNA™ miR-130a inhibitor (412568-00, Exiqon; Woburn, MA) or a scramble control (199004-00, Exiqon) was co-transfected (300 pmol) with the luciferase constructs.

2.6. Western Blotting

Murine hearts were harvested and protein lysates were prepared as previously described [24]. Total protein lysate was resolved by 4–20% SDS-PAGE transferred to a nitrocellulose membrane (Bio-Rad; Hercules, CA). Antibodies used: γ-Tubulin (T-6557, Sigma; St. Louis, MO), DSC2 (SC-66863, Santa Cruz; Dallas, TX), HRP-coupled goat anti-rabbit IgG (Jackson ImmunoResearch; West Grove, PA), and HRP-coupled goat anti-mouse (Jackson ImmunoResearch).

2.7. Immunofluorescence

Harvested hearts were frozen in Tissue-Tek OCT compound (Electron Microscopy Sciences). Frozen hearts were sectioned at 10 μm thickness and fixed with 100% methanol. Sections were then washed with phosphate buffered saline (PBS), and blocked in blocking buffer (PBS, 5% BSA, 0.2% Triton X-100) for 1 hour at room temperature. Sections were then incubated with rabbit anti-DSC2 (SC-66863, Santa Cruz) and goat anti-Plakoglobin antibody (SC-20466, Santa Cruz), followed by an Alexa-488-conjugated donkey anti-goat IgG antibody (A11008, Invitrogen; Carlsbad, CA) or Alexa-594-conjugated goat anti-rabbit IgG antibody (A11058, Invitrogen). Sections were mounted with VECTASHIELD® Mounting Media with DAPI (Vector Laboratories), and visualized with a Zeiss Axiophot fluorescence microscope. Images were merged using ImageJ software.

2.7.1. TUNEL Staining—Apoptotic cells were visualized *in situ via* terminal deoxynucleotidyl transferase-mediated nick end fluorescein labeling (TUNEL, Roche; Manheim, Germany). Frozen hearts were sectioned at 12 μm thickness and fixed with 4% PFA. Sections were rinsed in PBS and permeabilized in 0.1% Triton X-100/0.1% sodium citrate buffer. Sections were incubated in TUNEL reaction buffer for 1 hour at 37°C in a humidified chamber. Nuclei were counterstained with DAPI (VECTASHIELD®, Vector Laboratories)

2.8 Statistics

Values are reported as means ± SEM unless indicated otherwise. Student's t-test was used for comparing two means. Values of $p < 0.05$ were considered statistically significant. Statistical values were calculated using OriginPro software (OriginLab; Northampton, MA)

3. RESULTS

3.1. Adult Specific Expression of miR-130a Promotes RV Dilation and Ventricular Arrhythmogenesis

Using a tet-off αMHC bigenic expression system, our laboratory developed a transgenic mouse line capable of inducible overexpression of miR-130a in cardiomyocytes in the absence of doxycycline. On average, miR-130a is over-expressed in αMHC-miR130a cardiomyocytes at levels approximately 8-fold that of non-TG mice. Described previously by Osbourne *et al.*, αMHC-miR130a transgenic mice demonstrated progressive left ventricular dysfunction at 12 weeks after induction of miR-130a. We also found that there was a significant increase in ventricular arrhythmias αMHC-miR130a mice between 8 and 10 weeks off doxycycline (OD) [16].

In the present studies, we performed echocardiography in αMHC-miR130a and control littermate mice to determine the impact of mir-130a on right ventricular morphology. The endocardial dimensions were determined by tracing the area of the RV from a B-mode image obtained at end-diastole at the mid-venticular level. VisualSonics software was utilized to trace and calculate the right ventricular border at end-diastole (Fig. 1A). Images were obtained from 5 consecutive animals in each group at 10–12 weeks OD. In the αMHC-miR130a mice, the RV endocardial area was significantly increased compared with control

mice (CNTL 9.026 ± 0.28mm^2 vs. αMHC-miR130a 12.45 ± 1.2mm^2, $p<0.05$; Fig. 1B). However, there was no significant difference in RV wall thickness in these mice (data not shown).

Mice aged 8–10 weeks OD underwent arrhythmogenic screenings using surface ECG. Our results confirmed the presence of premature ventricular complexes (PVCs) in the αMHC-miR130a mice (11.52 ± 5.36 PVC/min), which validated our previously published findings. No PVCs were observed in age matched control mice (Fig. 1C, D). Previously, we showed that αMHC-miR130a mice can be induced into VT with electrical pacing at 6 weeks OD and are susceptible to spontaneous sustained VT at 10–12 weeks OD [16]. Here, we confirmed the onset of an arrhythmogenic phenotype (spontaneous; non-sustained) using non-invasive methodology. Once the arrhythmogenic phenotype was confirmed in the αMHC-miR130a mice (8–10 weeks OD), biochemical analysis was performed to determine DSC2 expression level.

3.2. DSC2 Expression is Downregulated in αMHC-miR130a Myocardium

To determine if miR-130a has a potential regulatory role on desmosome expression, we analyzed the 3′ UTRs of the major desmosomal and junction associated proteins that have been implicated in AC including: Plakophilin-2, Desmoplakin, Desmoglein-2, Desmocollin-2, Plakoglobin, and αT-catenin. Computational results from the microRNA database *rna22* [25] predicted target sites for miR-130a in the 3′UTR of Desmocollin 2 (DSC2) of both human and mouse. Of the investigated desmosomal proteins, the DSC2 3′ UTR yielded the only predicted target site for miR-130a (Fig. 2A). Therefore, DSC2 was a potential candidate for desmosomal regulation by miR-130a in our mouse model. DSC2 is an important desmosomal protein that has been shown to be dysregulated in human arrhythmogenic cardiomyopathy. To determine if DSC2 expression was affected in αMHC-miR130a mice, we performed immunofluorescent staining on tissue slides prepared from left ventricular free wall (LVFW), right ventricular free wall (RVFW), and septum. In the control myocardium, DSC2 is localized at the intercalated disc similar to that of the desmosomal protein Plakoglobin. Immunofluorescent staining showed significant loss of DSC2 expression in transgenic compared with littermate control hearts (Fig. 2B). To confirm these findings, western blot analysis for DSC2 from total protein lysates of ventricular myocardium was carried out. Densiometric analysis showed an ~80% reduction in mean DSC2 expression levels relative to age matched control mice (CNTL 3.42 ± 2.41 vs. αMHC-miR130a 0.74 ± 0.18; Fig. 2C, D).

3.3. Increased Fibrosis and Lipid Accumulation in αMHC-miR130a Myocardium

Clinically, histological findings of fibrofatty replacement of the myocardium is a hallmark feature of AC. Given the evidence for downregulation of DSC2, we set out to determine if αMHC-miR130a mice had evidence for fibrofatty infiltration in the ventricular myocardium. To investigate lipid accumulation, Oil red O staining was carried out on fresh myocardium sections from mice at 10 weeks OD (Fig. 3; upper panels). Lipid accumulation (stained in red) was observed in LVFW, RVFW, and the septum of αMHC-miR130a mice. Epicardial fat at the base was observed in both αMHC-miR130a and aged match control mice. However, only αMHC-miR130a mice had lipid accumulation within the myocardium. To

visualize fibrosis, ventricular myocardium sections were stained with Picro-Sirius Red. Areas of fibrosis (stained in red) were evident in miR-130a hearts at 10 weeks OD, whereas no fibrotic accumulation was visible in age matched control myocardium (Fig. 3; lower panel).

3.4. Increased Myocyte Cell Death in αMHC-miR130a Myocardium

Another prominent feature of AC is increased cardiomyocyte apoptosis. Here, we investigated differences in cell death within the ventricular myocardium of control and αMHC-miR130a mice using terminal deoxynucleotidyl transferase-mediated nick end fluorescein labeling (TUNEL) *in situ*. TUNEL staining was carried out on myocardium sections from mice at 10 weeks OD. As a counterstain, total nuclei visualized with DAPI (Fig. 4A). In αMHC-miR130a myocardium, a significantly elevated number of TUNEL-positive cells were observed compared to that of control myocardium (CNTL 0.87 ± 0.41% vs. αMHC-miR130a 12.23 ± 1.82%, $p<0.05$; Fig. 4B).

3.5. MiR-130a Acts as a Translational Repressor for DSC2 in 3T3 Cells

To validate DSC2 as a direct target of miR-130a, we performed *in vitro* target assays in NIH 3T3 fibroblasts, previously shown to express miR-130a [16]. Using a luciferase reporter, containing both firefly and renilla luciferase, we quantified relative repression levels of miR-130a on the 3′UTR of DSC2 compared with a negative control (SV40) 3′UTR. As shown in the schematic (Fig. 5A), the 3′UTRs are integrated within the firefly luciferase reading frame. The constructs were transfected in NIH 3T3 fibroblasts and luciferase expression levels were measured after 48 hours. Firefly luciferase expression was normalized to renilla luciferase, which was used as a measurement of transfection efficiency. The data presented (Fig. 5B) show the DSC2 3′UTR luciferase ratio relative to that of the negative control (normalized to 1). The 3T3 cells transfected with the DSC2 3′UTR had a significant reduction (~40%) in luciferase activity relative to control ($p<0.01$, $n=9$). This indicated that the DSC2 3′UTR was facilitating translation repression. To determine if the DSC2 3′UTR is a direct target of miR-130a, 3T3 cells were co-transfected with a LNA-antisense oligonucleotide that is designed to specifically block miR-130a. With miR-130a inhibition, translational repression was relieved by approximately 50%. As a negative control, scramble oligonucleotide was co-transfected with the luciferase constructs. Scramble oligonucleotide had no effect on translational repression. These results suggest miR-130a is acting directly as a translational repressor of DSC2.

4. DISCUSSION

AC, which is commonly referred clinically as ARVC/D, is now considered a more broad spectrum of disease that includes right (classical), left, and biventricular subtypes. Currently, clinical guidelines do not yet address the nonclassical variants and heterogeneity of the disease [26]. AC is most commonly associated with desmosomal dysfunction. However, it is important to note that mutations of desmosomal genes do arise in patients diagnosed with DCM that do not fit the histopathological criteria for AC [27]. Therefore, more studies are necessary to define the role of desmosomal dysfunction in both AC and DCM.

With an inducible transgenic mouse model, we demonstrated that overexpression of miR-130a in adult myocardium promotes ventricular arrhythmias and ventricular dysfunction. Using this mouse model and molecular assays, our lab previously described the regulation of connexin 43 by miR-130a [16]. The results from our previously published work show that gap junctions are diminished at the intercalated disc in myocardium overexpressing miR-130a. Given that desmosomes play an important role in intercalated disc function and morphology, we set out to investigate if miR130a regulates desmosomal expression. Based on computational alignment of the miR-130a sequence, the 3′UTR of DSC2 presents a predicted target site for miR-130a. Therefore, we hypothesized that overexpression of miR-130a in adult myocardium would promote downregulation of DSC2.

With IF and western blot analysis, we observe a significant decrease in DSC2 in αMHC-miR130a myocardium at 8–10 weeks OD. Although DSC2 expression was significantly decreased at the intercalated disc, it is interesting to note that variable DSC2 expression localized at the nucleus is observed (Fig. 2B). This could potentially be the result of truncated DSC2 expression or aberrant protein trafficking. The mechanism underlying nuclear DSC2 localization, however, remains to be elucidated.

In αMHC-miR130a transgenic mice, spontaneous ventricular arrhythmias always preceded the onset of LV dysfunction, which manifested itself at 12 weeks after miR-130a induction. Similar to connexin 43, decreased expression of DSC2 was evident before the onset of LV dysfunction. These results suggest that desmosomal dysfunction may also be playing a role in promoting a proarrhythmic substrate in these mice.

Desmosomal dysfunction is one of the major underlying causes for AC. Recent studies have proposed that decreased expression of desmosomal proteins is sufficient to facilitate the pathogenesis of AC [14, 15]. A major finding in AC due to desmosomal protein mutations is fibrofatty replacement within the myocardium. Our histological analysis of αMHC-miR130a transgenic mice show a significant increase in fibrosis and lipid accumulation within both LV and RV myocardium at 10 weeks after miR-130a induction. Increased cell death was also evident in the ventricular myocardium of these mice. Furthermore, we provide evidence for right ventricular dilation of mice 10–12 weeks OD. These findings support the hypothesis that reduction of desmosomal protein DSC2 by miR-130a overexpression is promoting desmosomal dysfunction, which likely contributes to the highly arrhythmogenic phenotype. It is possible that decreased DSC2 localization at the intercalated disc may occur secondary to the downregulation of connexin 43. However, our data from luciferase assays provide evidence for direct regulation of DSC2 by miR-130a. With the data provided from these experiments, we propose that miR-130a overexpression leads to dysregulation of the intercalated disc and a subsequent arrhythmogenic phenotype that resembles AC.

CONCLUSION

To our knowledge, no studies have described a Primary role for microRNAs in the pathogenesis of AC. Many desmosomal mutations have been described that promote the onset and progression of AC. More recently, it has been proposed that haploinsufficiency of desmosomal proteins is sufficient to promote AC. In this study, we present a highly

arrhythmogenic phenotype induced by miR-130a overexpression. Furthermore, we demonstrate that miR-130a is a direct regulator of DSC2. These novel findings highlight a potential role for miR-130a in promoting desmosomal dysfunction. Moreover, the histological findings of αMHC-miR130a myocardium are reminiscent of those seen in the other models of desmosomal protein loss. In conclusion, overexpression of miR-130a results in a disease phenotype resembling AC and therefore, may serve as potential model for microRNA-induced AC.

Acknowledgments

Declared none.

References

1. Calore M, Lorenzon A, De Bortoli M, Poloni G, Rampazzo A. Arrhythmogenic cardiomyopathy: a disease of intercalated discs. Cell Tissue Res. 2015; 360(3):491–500. [PubMed: 25344329]
2. Saguner AM, Brunckhorst C, Duru F. Arrhythmogenic ventricular cardiomyopathy: A paradigm shift from right to biventricular disease. World J Cardiol. 2014; 6(4):154–74. [PubMed: 24772256]
3. Basso C, Bauce B, Corrado D, Thiene G. Pathophysiology of arrhythmogenic cardiomyopathy. Nat Rev Cardiol. 2012; 9(4):223–33.
4. Sen-Chowdhry S, McKenna WJ. Sudden Death from Genetic and Acquired Cardiomyopathies. Circulation. 2012; 125:1563–76. [PubMed: 22451606]
5. Sen-Chowdhry S, Syrris P, Prasad SK, et al. Left-dominant arrhythmogenic cardiomyopathy: an under-recognized clinical entity. J Am Coll Cardiol. 2008; 52(25):2175–87. [PubMed: 19095136]
6. Rigato I, Bauce B, Rampazzo A, et al. Compound and digenic heterozygosity predicts lifetime arrhythmic outcome and sudden cardiac death in desmosomal gene-related arrhythmogenic right ventricular cardiomyopathy. Circ Cardiovasc Genet. 2013; 6(6):533–42. [PubMed: 24070718]
7. Basso C, Thiene G, Corrado D, Angelini A, Nava A, Valente M. Arrhythmogenic right ventricular cardiomyopathy. Dysplasia, dystrophy, or myocarditis? Circulation. 1996; 94(5):983–91. [PubMed: 8790036]
8. Basso C, Corrado D, Marcus FI, Nava A, Thiene G. Arrhythmogenic right ventricular cardiomyopathy. Lancet. 2009; 373(9671):1289–300. [PubMed: 19362677]
9. Murray B. Arrhythmogenic right ventricular dysplasia/cardiomyopathy (ARVD/C): a review of molecular and clinical literature. J Genet Couns. 2012; 21(4):494–504. [PubMed: 22426942]
10. Sheikh F, Ross RS, Chen J. Cell-cell connection to cardiac disease. Trends Cardiovasc Med. 2009; 19(6):182–90. [PubMed: 20211433]
11. Lyon RC, Mezzano V, Wright AT, et al. Connexin defects underlie arrhythmogenic right ventricular cardiomyopathy in a novel mouse model. Hum Mol Genet. 2014; 23(5):1134–50. [PubMed: 24108106]
12. Delmar M, McKenna WJ. The cardiac desmosome and arrhythmogenic cardiomyopathies: from gene to disease. Circ Res. 2010; 107(6):700–14. [PubMed: 20847325]
13. Rasmussen TB, Nissen PH, Palmfeldt J, et al. Truncating plakophilin-2 mutations in arrhythmogenic cardiomyopathy are associated with protein haploinsufficiency in both myocardium and epidermis. Circ Cardiovasc Genet. 2014; 7(3):230–40. [PubMed: 24704780]
14. Asimaki A, Tandri H, Huang H, et al. A new diagnostic test for arrhythmogenic right ventricular cardiomyopathy. N Engl J Med. 2009; 360(11):1075–84. [PubMed: 19279339]
15. Vite A, Gandjbakhch E, Prost C, et al. Desmosomal cadherins are decreased in explanted arrhythmogenic right ventricular dysplasia/cardiomyopathy patient hearts. PLoS One. 2013; 8(9):e75082. [PubMed: 24086444]
16. Osbourne A, Calway T, Broman M, McSharry S, Earley J, Kim GH. Downregulation of connexin43 by microRNA-130a in cardiomyocytes results in cardiac arrhythmias. J Mol Cell Cardiol. 2014; 74:53–63. [PubMed: 24819345]

17. Kim GH. MicroRNA regulation of cardiac conduction and arrhythmias. Transl Res. 2013; 161(5): 381–92. [PubMed: 23274306]
18. Ambros V. The funtions of animal microRNAs. Nature. 2004; 431(7006):350–5. [PubMed: 15372042]
19. Thum T, Galuppo P, Wolf C, et al. MicroRNAs in the human heart: a clue to fetal reprogramming in heart failure. Circulation. 2007; 116(3):258–67. [PubMed: 17606841]
20. Matkovich SJ, Van Booven DJ, Youker KA, et al. Reciprocal regulation of myocardial microRNAs and messenger RNA in human cardiomyopathy and reversal of the microRNA signature by biomechanical support. Circulation. 2009; 119(9):1263–71. [PubMed: 19237659]
21. Calway T, Bak T, Kim GH. MicroRNA Expression Pattern in Patients with Ventricular Tachycardia and End-Stage Heart Failure. J Heart Lung Trans. 2015; 34(4):S272–3.
22. Lorenzon A, Pilichou K, Rigato I, et al. Homozygous Desmocollin-2 Mutations and Arrhythmogenic Cardiomyopathy. Am J Cardiol. 2015; 116(8):1245–51. [PubMed: 26310507]
23. Gehmlich K, Lambiase PD, Asimaki A, et al. A novel desmocollin-2 mutation reveals insights into the molecular link between desmosomes and gap junctions. Heart Rhythm. 2011; 8(5):711–8. [PubMed: 21220045]
24. Kim GH, Samant SA, Earley JU, Svensson EC. Translational control of FOG-2 expression in cardiomyocytes by micro-RNA-130a. PLoS One. 2009; 4(7):e6161. [PubMed: 19582148]
25. Miranda KC, et al. A pattern-based method for the identification of MicroRNA binding sites and their corresponding heteroduplexes. Cell. 2016; 126:1203–1217.
26. Marcus FI, McKenna WJ, Sherrill D, et al. Diagnosis of Arrhythmogenic Right Ventricular Cardiomyopathy/Dysplasia. Circulation. 2010; 121:1533–41. [PubMed: 20172911]
27. Garcia-Pavia P, Syrris P, Salas C, et al. Desmosomal protein gene mutations in patients with idiopathic dilated cardiomyopathy undergoing cardiac transplantation: a clinicopathological study. Heart. 2011; 97:1744–52. [PubMed: 21859740]

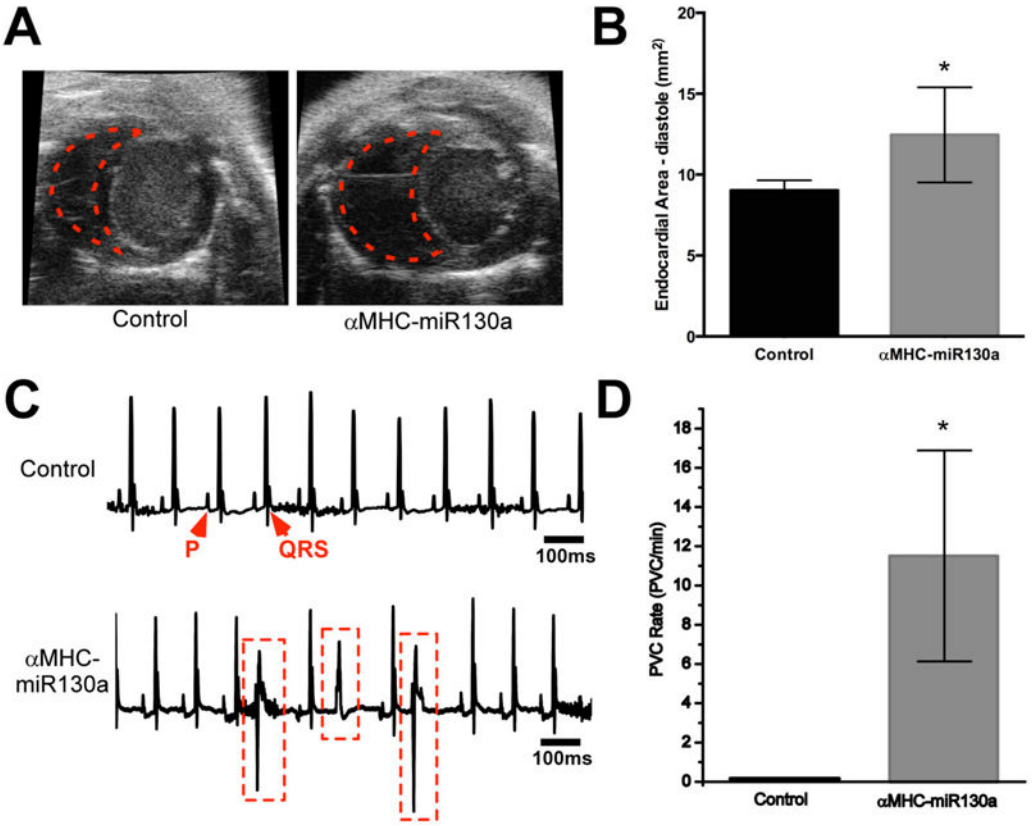

Fig. 1.

miR-130a Promotes RV Dilation and Ventricular Arrhythmogenesis. (**A**) Representative echocardiography B-mode images at the mid-ventricular level of control and αMHC-miR130a hearts. Endocardial dimensions of the RV at end diastole are traced (red). (**B**) Average RV endocardial area for control and αMHC-miR130a hearts (n=5 mice per group; $p<0.05$) Cardiac Arrhythmogenesis and RV dilation in αMHC-miR130a Mice. (**C**) Representative surface ECG of control vs. αMHC-miR130a mouse 8 weeks off doxycycline. αMHC-miR130a mice exhibit premature ventricular complexes while age matched control mice maintain a normal sinus rhythm. (**D**) PVC propensity quantified for both groups ($p<0.01$; CNTL, n=14; αMHC-miR130a, n=17).

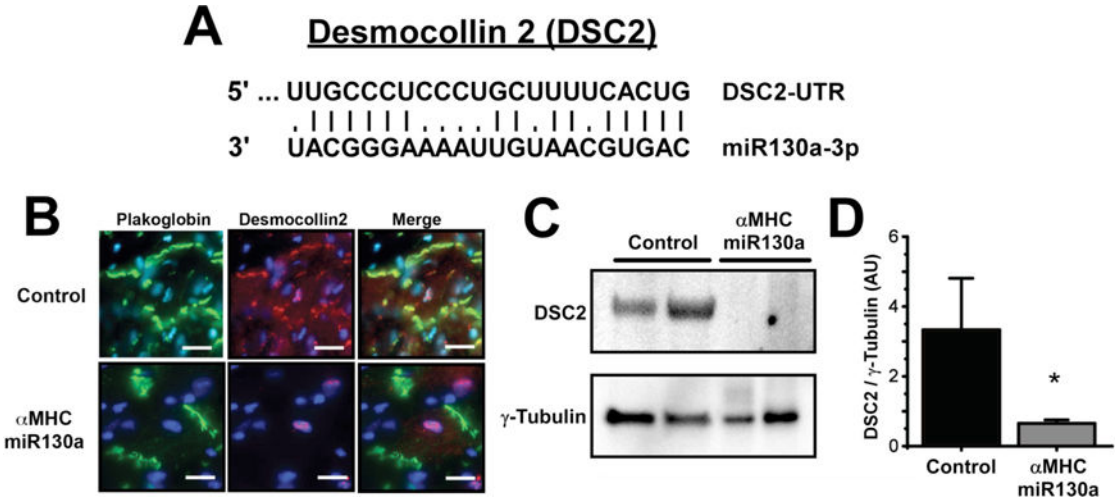

Fig. 2.

Reduced Desmocollin-2 Protein Levels in Cardiomyocytes Overexpressing miR-130a. (**A**) Computational alignment of potential target site in the Desmocollin-2 3′UTR and miR-130a. (**B**) Representative immunofluorescent staining of Desmocollin-2 and Plakoglobin (localized at the intercalated disc) taken from LV myocardium of aMHC-miR130a mice 10 weeks OD compared with age matched control (scale bar = 10μm). Loss of Desmocollin-2 was evident in aMHC-miR130a mice 8–10 weeks off doxycycline. Nuclei are counterstained with DAPI. (**C**) Western blot analysis using total protein of ventricular myocardium from mice 8–10 weeks off doxycycline was performed for Desmocollin-2 with γ-Tubulin used as a loading control. (**D**) Densitometric analysis of Desmocollin-2 (DSC2) from non-transgenic myocardium compared with miR-130a transgenic myocardium shows ~80% reduction in protein expression. (n=4 mice per group; $p<0.05$).

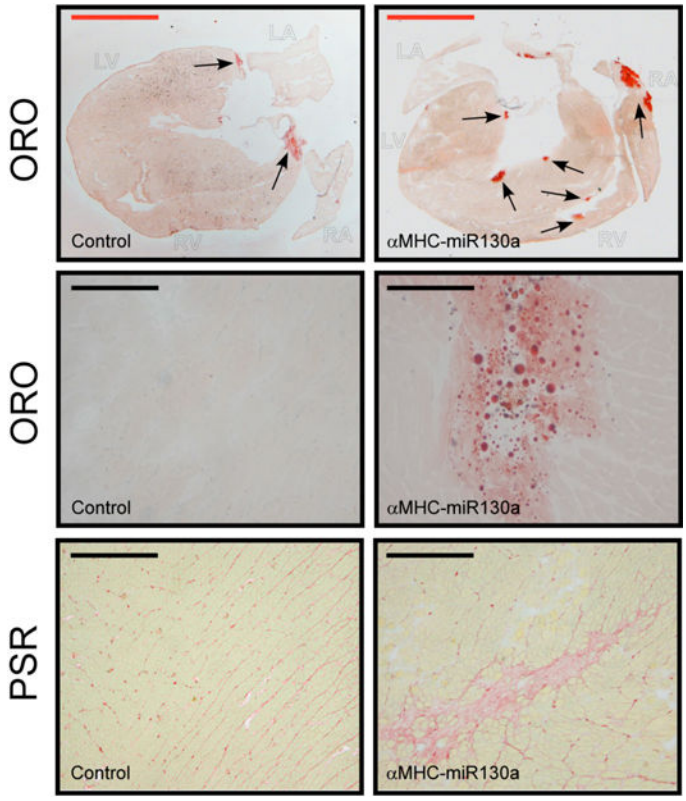

Fig. 3.

Evidence for Fibrosis and Lipid Accumulation in αMHC-miR130a Mice. Representative myocardium sections stained with Oil Red O from control and aMHC-miR130a mice (ORO; Top). Representative LVFW section image at 20× (ORO; Middle) at 10 weeks off doxycycline. Evidence for lipid accumulation is proven by the presentation of red lipid droplets within the myocardium. Representative ventricular myocardium sections (LVFW pictured) stained with Picro-Sirius Red from control and aMHC-miR130a mice (PSR; Bottom) at 10 weeks off doxycycline. Accumulation of fibrosis stained in red is evident in aMHC-miR130a myocardium. (Scale bar; red = 3mm, black = 100μm).

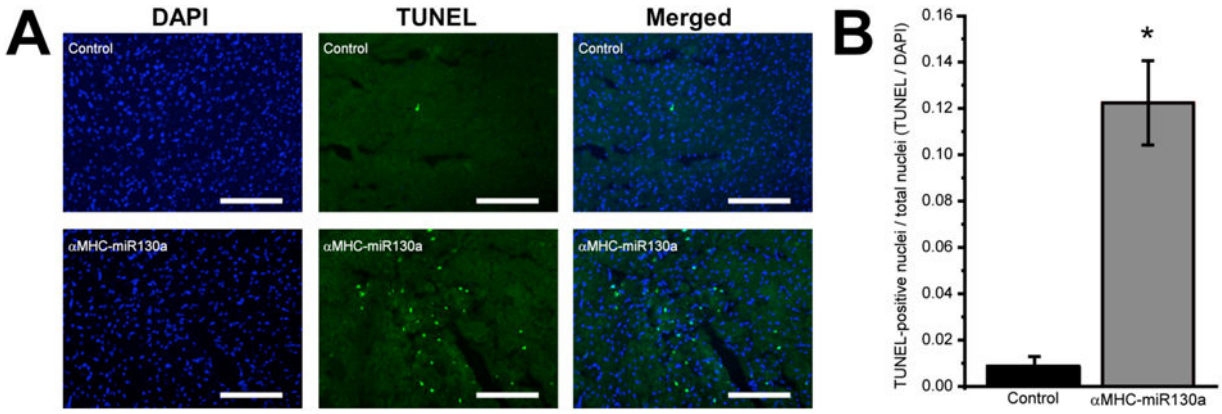

Fig. 4.

Increased Cell Death in αMHC-miR130a Myocardium. Representative ventricular myocardium sections stained with TUNEL and DAPI (scale bar = 100μm; **A**). TUNEL-positive nuclei were quantified as a ratio of total visible nuclei, which are counterstained by DAPI (n=3 per group, 4 images for each heart; $p<0.01$; **B**).

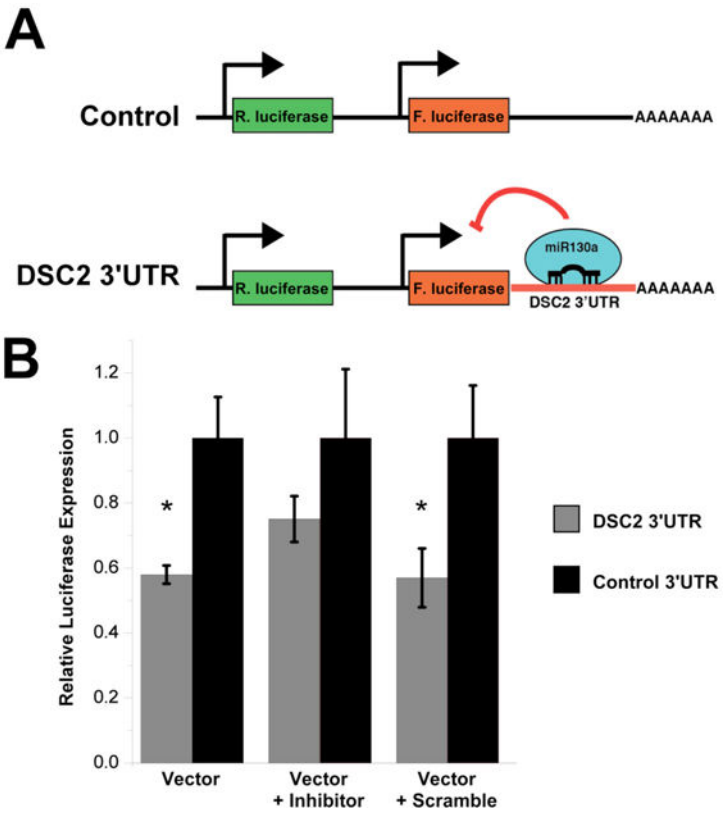

Fig. 5.

Desmocollin-2 3′UTR is a Target for MicroRNA Regulation of Gene Expression. (**A**) To determine if the Desmocollin-2 3′UTR is potential target site for microRNA regulation, a luciferase expression construct was generated so that the 3′UTR was incorporated into the Renilla luciferase mRNA. Firefly luciferase is included as a transfection control. Luciferase constructs were transfected in 3T3 fibroblast cells, which are known to express miR-130a. Constructs were co-transfected with miR-130a inhibitor or scramble to determine contribution of miR-130a (**B**) Renilla and Firefly luciferase expression was quantified in triplicate for each transfection using fluorometric analysis and is presented as a ratio of Renilla relative to Firefly luciferase expression ($p<0.01$, n=9 transfections per group).